

Short Communication

Corrosion behaviour of S500AW railway steel in a simulated industrial atmospheric environment

Hao Zhang¹, Jialiang Song¹, Zhaoliang Li¹, Junhang Chen¹, Wei Yu², Chenghui Yin¹,
Chaofang Dong¹ and Kui Xiao^{1,*}

¹ Institute for Advanced Materials and Technology of University, Science and Technology Beijing, Beijing 100083, China

² Engineering Research Institute, University of Science and Technology Beijing, Beijing 100083, China

*E-mail: xiaokui@ustb.edu.cn

Received: 23 May 2022 / Accepted: 19 July 2022 / Published: 7 August 2022

The corrosion behaviours of Q345B carbon steel and S500AW railway steel for railways were evaluated in a simulated industrial atmosphere, and the corrosion mechanism of S500AW railway steel was explored. Periodic immersion corrosion experiments were carried out on two types of steel, and the experimental periods were divided into 24 h, 120 h, 240 h and 360 h. The corrosion weight loss and corrosion rate were calculated by the weight loss method. The corrosion potentials and corrosion current densities of the two types of steel in four cycles were analysed by electrochemical experiments. The macromorphology, micromorphology and corrosion product composition were analysed to evaluate the corrosion behaviour of Q345B and S500AW. The corrosion rate of S500AW in the periodic immersion corrosion experiments was lower than that of Q345B. With an extension of the experiment time, the proportion of α -FeOOH in the rust layer increased. In the simulated industrial atmosphere, the corrosion resistance of S500AW was better than that of Q345B. During the 360-h immersion experiments, the value of α/γ of Q345B increased at first and then appears to be steady, while the α/γ value of S500AW continued to increase.

Keywords: Steel for train body; Industrial atmospheric corrosion; Periodic immersion test; Rust layer structure; Rust layer composition

1. INTRODUCTION

In recent years, China's railway system has been in a period of rapid development. With the expansion of the scale and coverage of the railway network, the railway possesses an important position in freightage enterprises. The data in the *Railway Statistical Bulletin 2020* indicate that the total freight volume improved by 3.2% over the previous year and put forward the requirements of heavy load, high speed and safety for freight trains to fulfil the low cost, environmental friendliness and overall efficiency

improvement of rail transit throughout its life cycle 1-3. To meet the conditions of atmospheric corrosion resistance, Chinese railway freight train steel has gone through several stages including carbon steel (Q235, etc.), low alloy steel (09Mn2 Series), weathering steel (09CuPTiRE, 09CuPCrNi, etc.) and high-strength weathering steel (Q450NQR1, S500AW, etc.) 4-5.

In a realistic industrial atmospheric environment, railway freight trains are eroded by corrosive pollutants such as SO_2 , CO_2 , chloride and dust 6, leading to accelerated steel corrosion. Yin et al. found that Cu and Cr alloy elements in high-strength weathering steel participate in corrosion film formation, which can enhance the compactness of the film 7. Liu et al. researched the corrosion of V-N-8Cr weathering steel. They found that uneven stress accumulation causes microcracks in the corrosion rust layer during the corrosion process. At the same time, Cr could promote the formation of chromium oxide and $\alpha\text{-FeOOH}$ to repair defects 8. Zhang et al. studied the role of P, Cu and other elements in the atmospheric corrosion of weathering steel and found that P oxidises to PO_4^{3-} , which can be used as a corrosion inhibitor to decrease the anodic dissolution rate. In addition, the formation of CuO can fill the defects in the corrosive rust layer and improve the corrosion resistance 9. Qian et al. found that the rust layer of Q345qD was formed by $\alpha\text{-FeOOH}$ and a large amount of $\gamma\text{-Fe}_2\text{O}_3\cdot\text{H}_2\text{O}$, while the rust layer of Q450NQR1 highly strengthened weathering steel consisted of a single $\alpha\text{-FeOOH}$ component 10, which is similar to the results demonstrated by K. Asami et al. 11. Fu et al. examined the atmospheric corrosion of the rust layer of weathering steel and found that the alloying elements in the rust layer can promote the transformation of $\gamma\text{-FeOOH}$ to $\alpha\text{-FeOOH}$ 12. Qian et al. found that the Cr element in weathering steel can promote the formation of a defensive rust layer and enhance the passivation ability of weathering steel, so it can improve the atmospheric corrosion resistance 13. Zhang et al. believed that there is no difference in the phase composition of the interior and exterior rust layers of carbon steel, while the proportion of the amorphous phase in the interior rust layer of weathering steel is higher than that of the exterior rust layer 14. Yu et al. studied the influence of Cr on the corrosion behaviour of weathering steel and found that Cr can form FeCr_2O_4 in the rust layer, improving the atmospheric corrosion resistance 15. Liu et al. believed that the enrichment of chromium in weathering steel promotes the formation of a protective rust layer, which acts as a barrier to prevent the corrosion process 16. Wang et al. found that the interior rust layer of weathering steel consists of an amorphous phase and $\alpha\text{-FeOOH}$ nanoparticles, the exterior rust layer is mainly rod-shaped $\gamma\text{-FeOOH}$, and Cr is enriched in the amorphous phase of the interior rust layer 17. The atmospheric corrosion resistance of weathering steel is generally considered to be the effect of weathering elements (mainly Cr) and the shielding and blocking effect on corrosive media of the tight interior rust layer dominated by $\alpha\text{-FeOOH}$ 18-20.

However, there are few studies on the corrosion resistance of S500AW steel for railway freight trains and the influence of the composition of corrosion products on the corrosion resistance in a simulated industrial atmospheric environment. In this paper, the growth rate and upper limit of the α/γ values of the corrosion products of Q345B and S500AW and the corrosion mechanism of S500AW railway steel were analysed and studied through 360-h periodic immersion experiments under simulated industrial atmospheric conditions. The corrosion kinetics of the two types of steel were studied by the weight-loss method, the corrosion product structures and components of the two types of steel were evaluated and analysed by scanning electron microscope (SEM) and X-ray diffraction (XRD), and the electrochemical characteristics of the two types of steel were analysed by potentiodynamic polarization

curves. The rust layer composition and the defensive effect of the structure on the metal substrate were studied, which provided a reference for the use of freight train body steel in the industrial atmospheric environment.

2. EXPERIMENTAL PROCEDURES

2.1. Materials

The tested steel used in this paper is Q345B carbon steel and S500AW railway steel. The chemical compositions of the two types of steel are listed in Table 1.

The specimens were cut to dimensions of 50 mm×25 mm×3 mm for the periodic immersion experiments. The cut samples were polished to 800 mesh, washed and dehydrated with absolute ethanol, dried and stored. A Vernier calliper was used to measure and record the original size of the samples, and a balance with an accuracy of not less than 0.1 mg was used to weigh and record the original weight of the specimens.

Table 1 Chemical composition of experimental steel, wt.%

Material	C	Si	Mn	Cr	Ni	Cu	Sb	Nb	Fe
Q345B	0.17	0.09	0.35	0.03	0.04	0.01	<0.0001	<0.001	rest
S500AW	0.06	0.20	0.64	0.88	0.20	0.29	0.079	0.025	

2.2. Periodic Immersion Experiments

Q345B and S500AW specimens were subjected to periodic immersion corrosion experiments for 24 h, 120 h, 240 h and 360 h. The experimental environment was 0.01 mol/L NaHSO₃, and the experimental temperature was 25 °C. During the tests, each cycle time was 60 min, of which the soaking time was 12 min, and the solution temperature was 45 °C. The drying time was 48 min, the drying temperature was 70 °C, and the humidity in the test chamber during the drying period was less than 30%. Make-up solution was added every 72 h, and the make-up solution was 0.02 mol/L NaHSO₃ to keep the solution composition in the experimental chamber unchanged.

The corrosion rates of the two materials after different cycles were calculated by the weight loss method. The calculation formula is as follows:

Weight loss:

$$\Delta w = \frac{m_0 - m_1}{A} \quad (1)$$

Weight loss rate:

$$v = \frac{m_0 - m_1}{At} \quad (2)$$

where Δm is the weight loss (g); m_0 and m_1 are the initial weight and weight after removing surface rust, respectively (g); A is the superficial area of the specimens (m²); v is the corrosion rate of the samples (g·m⁻²·s⁻¹); and t is the test time (h).

The corrosion kinetics law was obtained by fitting the above corrosion data. The corrosion weight loss of low alloy steel in the atmospheric environment generally follows the power function law 21, as shown below:

$$\Delta w = Dt^n \quad (3)$$

where t is the experiment time (h), and D and n are constants. The value of D can reflect the corrosion rate of the materials. The value of n can be used to evaluate the protective strength of the rust layer. Generally, the value of n is between 0.5~1.0. The closer it is to 0.5, the better the protection of the rust layer 22.

The samples were derusted with a derusting solution at the end of each cycle. The derusting solution was made by mixing 500 ml hydrochloric acid, 3.5 g hexamethylene tetramine and 500 ml water. The derusting solution on the surface of the specimens was rinsed with deionized water, dehydrated with absolute ethanol, dried with a blower, and stored in a drying oven for 24 hours. Three parallel samples were taken from each group, and a balance with an accuracy of not less than 0.0001g was used to weigh and record the samples.

2.3 Potentiodynamic polarization test

Q345B and S500AW samples were removed at 24 h, 120 h, 240 h and 360 h of the periodic immersion experiment, and their potentiodynamic polarization curves were tested with a Parstat 4000 electrochemical workstation. The sample is used as the working electrode (WE), saturated calomel electrode (SEC) as the reference electrode (RE), and platinum as the auxiliary electrode (AE). The test environment was a 0.01 mol/l NaHSO₃ solution, and the test temperature was 25 °C. An open-circuit potential (OCP) test was conducted in the 2000s to ensure that the system reached stability. The action potential polarization curve was tested in a range of OCP ± 0.5 V at a scanning rate of 0.5 mV/s. By Tafel extrapolation [23], the corrosion potential and corrosion current density of the samples in different cycle periods were obtained.

2.4 Surface Topography of Layer of Rust

A Nikon D7000 digital camera was used to record the corrosion macromorphology of the surface of the specimens. An FEI Quanta 250 scanning electron microscope (SEM) was used to observe the corrosion micromorphology of the surface of the specimens and the micromorphology of the sections, and the corrosion products were analysed by energy dispersive spectroscopy (EDS).

2.5 Composition Analysis of Corrosion Products

The corrosion products were scanned in the range of 10° ~ 90° with an Ultima IV XRD analyser at a scanning rate of 4°/min. The relative contents of the phase in the rust layer were determined semiquantitatively by comparing the XRD intensity of different samples.

3. RESULTS

3.1 Weight loss measurements

Figure 1 shows the relationship between the corrosion weight loss and experimental cycles in 0.01 mol/L NaHSO₃ at 25 °C. In the simulated industrial environment, the corrosion weight loss of the two types of steel increases with the extension of the test cycle, but the growth rate of the weight loss of the two types of steel is different. The growth rate of Q345B carbon steel is significantly higher than that of S500AW railway steel. The weight loss of S500AW railway steel is much lower than that of Q345B carbon steel under the same experimental cycles.

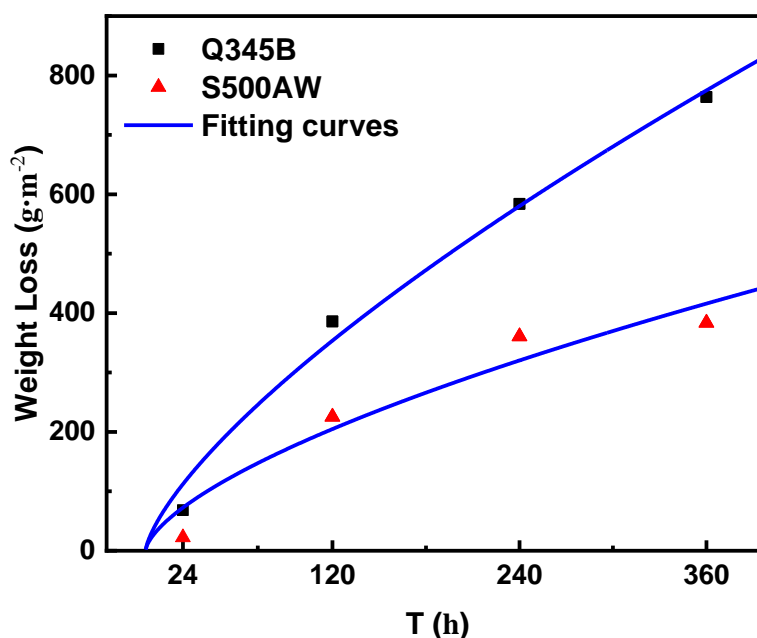


Figure 1 Weight loss and kinetic fitting curves of experimental steel after different periodic immersion tests in 0.01 mol/L NaHSO₃ at 25 °C.

Table 2 details the corrosion rate and annual corrosion rate of the two types of steel after different periodic immersion tests in 0.01 mol/L NaHSO₃ at 25 °C. It can be seen from the results in Table 2 that the maximum corrosion weight loss of Q345B carbon steel is 3.04 times that of S500AW railway steel at 24 h. The corrosion rate of the two types of steel first increased and then decreased with the extension of the experimental period. The corrosion rate was the highest at 120 h, and the corrosion rate showed a gradual downward trend after 120 h. The corrosion rate of S500AW railway steel was significantly lower than that of Q345B carbon steel under the same test cycles. It can be seen from the results in

Table 2 that the maximum corrosion rate and annual corrosion rate of Q345B carbon steel were 2.95 times those of S500AW railway steel at 360 h.

Table 2 Corrosion rate and annual corrosion rate of two types of steel after different periodic immersion tests in 0.01 mol/L NaHSO₃ at 25 °C.

Test times (h)	Corrosion rate (g/(m ² ·h))		Annual corrosion rate (mm/a)	
	Q345B	S500AW	Q345B	S500AW
	24	2.5258	1.1433	2.8150
120	4.2293	1.8778	4.7136	2.0928
240	3.6348	1.5448	4.0510	1.7217
360	3.5232	1.1955	3.9664	1.3324

The blue curves in Figure 1 are the fitting results. The corrosion weight loss of the two types of steel conformed to the law of $\Delta w = Dt^n$. The fitting parameters are listed in Table 3. The D value of Q345B carbon steel was greater than that of S500AW railway steel in the simulated industrial atmospheric environment, which indicated that the corrosion rate of Q345B carbon steel is greater than that of S500AW railway steel at the initial stage of corrosion. In addition, the n values in the fitting results of corrosion weight loss of the two types of steel were less than 1.0, indicating that the rust layer formed has a certain protective function. The n value of S500AW railway steel was the smallest and closer to 0.5 in the fitting values of the two types of steel, implying that the corrosion product rust layer formed by S500AW railway steel had stronger atmospheric corrosion resistance and protection than Q345B carbon steel.

Table 3 Fitting parameters of corrosion weight loss of experimental steel.

Materials	D	n	R^2
Q345B	11.60718	0.71372	0.98835
S500AW	9.35365	0.64473	0.93184

3.2 Corrosion Morphology

Figure 2 and Figure 3 present the corrosion macromorphology of Q345B carbon steel and S500AW railway steel after periodic immersion experiments for different numbers of cycles, respectively. Yellowish-brown corrosion products were produced on the surface of the two types of steel after 24 h. The surface colour of the two kinds of steel deepened and gradually turned brown after 120 h. The change in the Q345B carbon steel is the most obvious. It is noted that the rust layer on the surface of the Q345B carbon steel samples is thin and discontinuous, and the substrate is exposed to the experimental environment. Therefore, at this stage, the corrosion rate of Q345B carbon steel is very fast, and the corrosion rate reaches the peak of all experiments. The corrosion of the specimens is aggravated, the surface becomes a rough spherical cluster, and a small amount of dark brown substances are scattered on the surface of Q345B carbon steel at 240 h. After 360 h of the test, it can be observed that the surface of Q345B carbon steel presents a dark brown substrate due to the peeling off of corrosion products, while the surface of S500AW railway steel is relatively complete, and the surface of the sample presents a yellowish-brown.

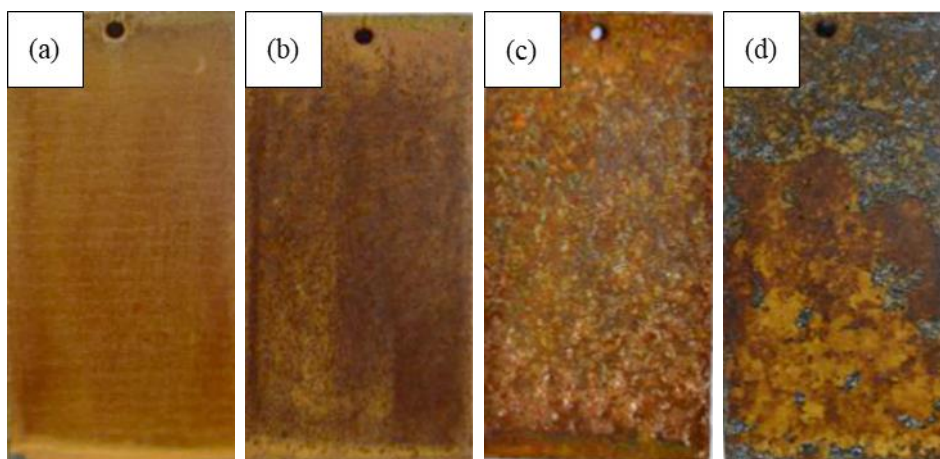


Figure 2 Corrosion macromorphology of Q345B carbon steel at specific experimental times, environments and temperatures: (a) 24 h, 0.01 mol/L NaHSO₃, 25 °C; (b) 120 h, 0.01 mol/L NaHSO₃, 25 °C; (c) 240 h, 0.01 mol/L NaHSO₃, 25 °C; (d) 360 h, 0.01 mol/L NaHSO₃, 25 °C.

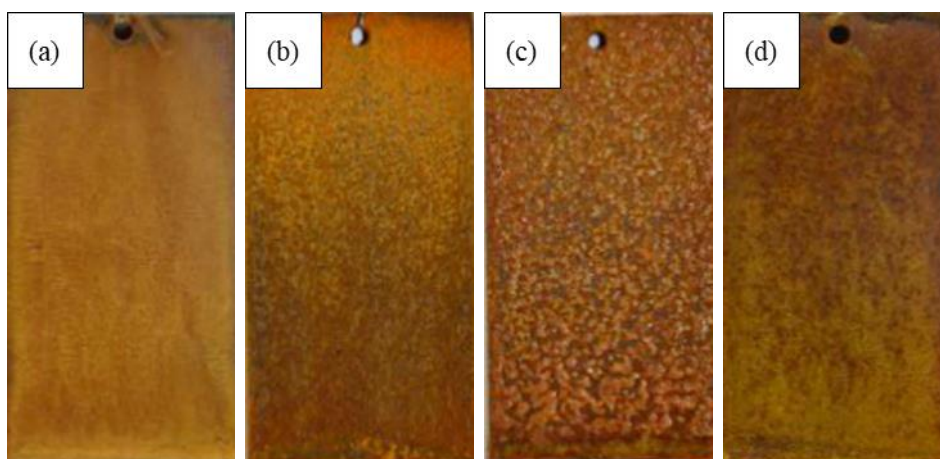


Figure 3 Corrosion macromorphology of S500AW at specific experiment times, environments and temperatures: (a) 24 h, 0.01 mol/L NaHSO₃, 25 °C; (b) 120 h, 0.01 mol/L NaHSO₃, 25 °C; (c) 240 h, 0.01 mol/L NaHSO₃, 25 °C; (d) 360 h, 0.01 mol/L NaHSO₃, 25 °C.

Figure 4 and Figure 5 display the micromorphology of Q345B carbon steel and S500AW railway steel, respectively, after periodic immersion experiments for different numbers of cycles. After 24 h of the experiment, the surfaces of the two types of steel were covered with flocculent corrosion product γ -FeOOH₂₄, and there were cracks, pores and other defects between the granular products on the surface of the Q345B carbon steel. Meanwhile, the microscopic granular flocculent products on the surface of the S500AW railway steel were smaller, and there were no obvious cracks, pores or other defects. With the extension of the experimental time, the corrosion products on the surface of the sample gradually became dense after 120 h and 240 h. Figure 5 (d) indicates a large number of cluster products on the surface of S500AW railway steel, which is generally considered to be α -FeOOH. Cluster corrosion products were also found on the surface of Q345B carbon steel. The subsequent dense corrosion products

gradually filled the cracks, pores and other defects of the previous corrosion products, and almost all defects of the rust layer of S500AW railway steel were filled after 360 h of the test. Moreover, through a comparison of the two types of steel samples, it was found that the corrosion product particles on the surface of Q345B carbon steel were larger, while the corrosion product particles of S500AW railway steel were relatively smaller.

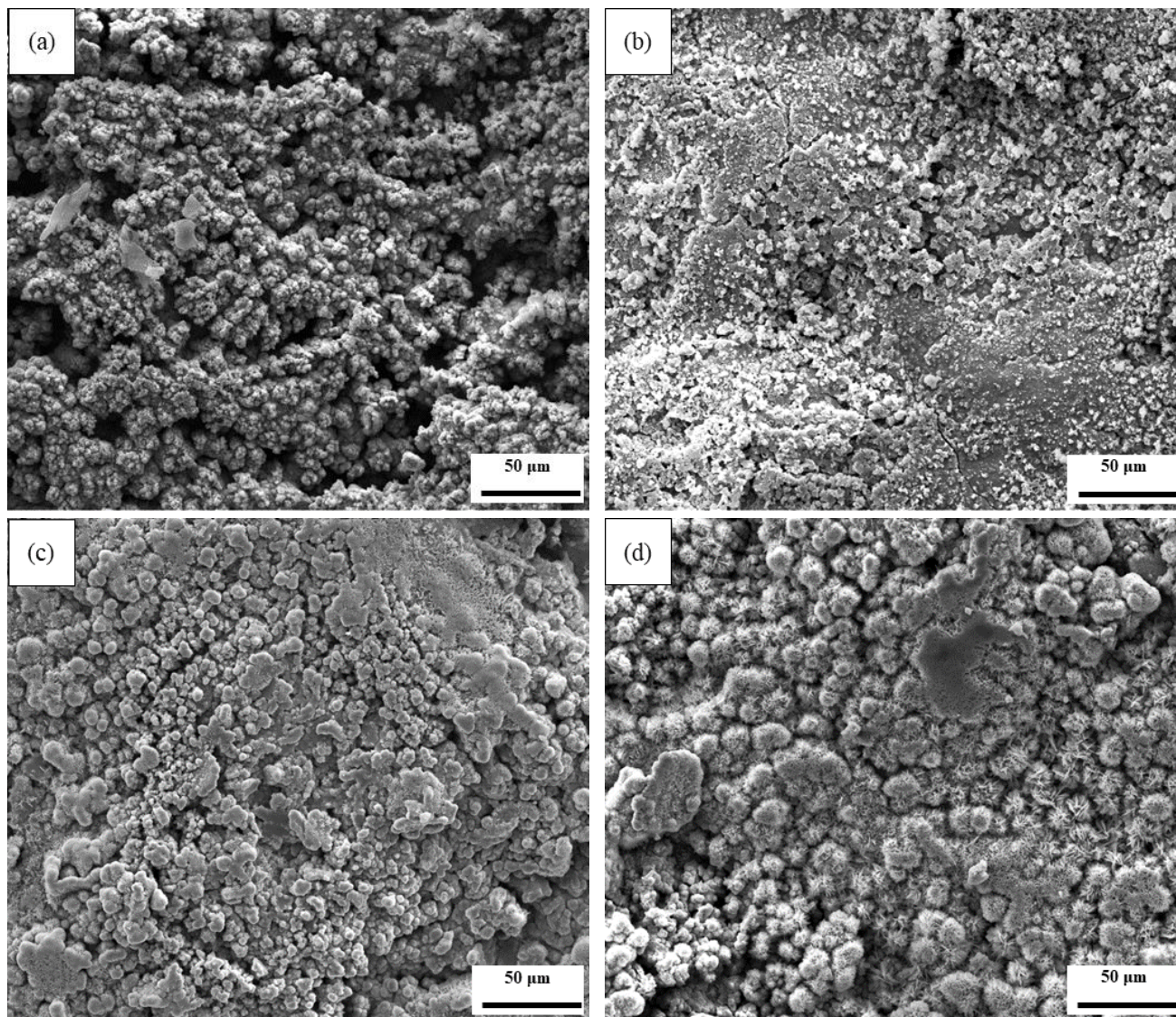


Figure 4 SEM images of Q345B carbon steel at specific experiment times, environments and temperatures: (a) 24 h, 0.01 mol/L NaHSO₃, 25 °C; (b) 120 h, 0.01 mol/L NaHSO₃, 25 °C; (c) 240 h, 0.01 mol/L NaHSO₃, 25 °C; (d) 360 h, 0.01 mol/L NaHSO₃, 25 °C.

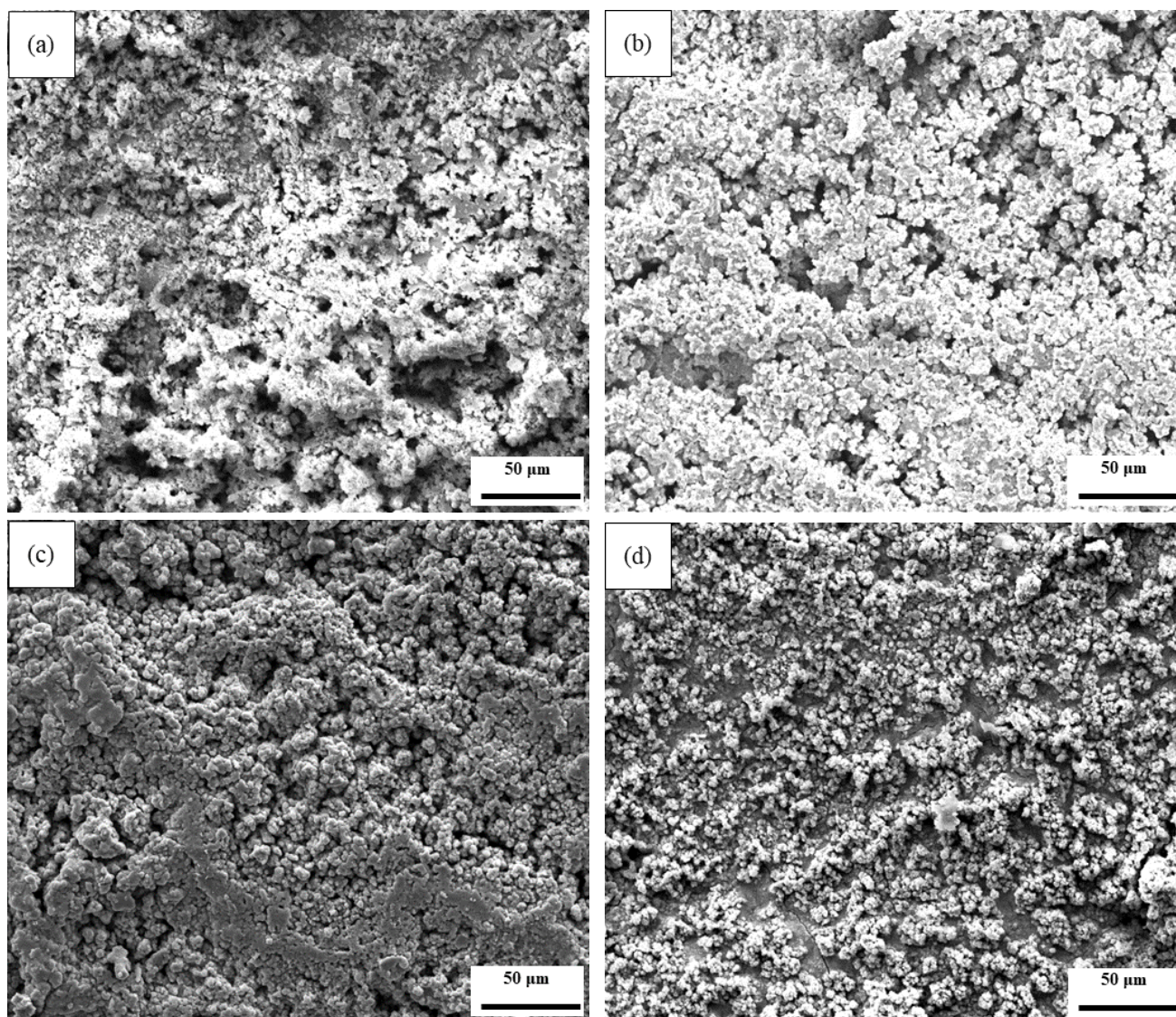


Figure 5 SEM images of S500AW railway steel at specific experiment times, environments and temperatures: (a) 24 h, 0.01 mol/L NaHSO₃, 25 °C; (b) 120 h, 0.01 mol/L NaHSO₃, 25 °C; (c) 240 h, 0.01 mol/L NaHSO₃, 25 °C; (d) 360 h, 0.01 mol/L NaHSO₃, 25 °C.

To further explore the corrosion resistance mechanism of S500AW railway steel, the cross-section rust layers of two types of steel after 360-h peripheral immersion experiments were analysed. Figure 6 and Figure 7 present the sectional morphology and element distribution of the rust layer of Q345B carbon steel and S500AW railway steel after 360 h, respectively.

It can be illustrated from the cross-section SEM images that the corrosion products of S500AW railway steel are denser than those of Q345B carbon steel. The rust layer of Q345B carbon steel has large longitudinal and transverse cracks and many small microcracks. However, the rust layer of S500AW railway steel has interior and exterior structures: the exterior rust layer has micropores and cracks, which are relatively loose, while the interior rust layer is relatively dense, which can provide a defensive function for steel 25. In addition, in terms of element distribution, Q345B carbon steel has no corrosion-resistant element Cr, but there is Cr at the interior and exterior interfaces of the rust layer and the substrate of the weathering steel, and the enrichment of Cr is mainly concentrated in the interior rust

layer. S is widely distributed and densely distributed in Q345B carbon steel. The distribution of S can also be observed on the substrate, while the distribution of S in S500AW railway steel is sparse and low.

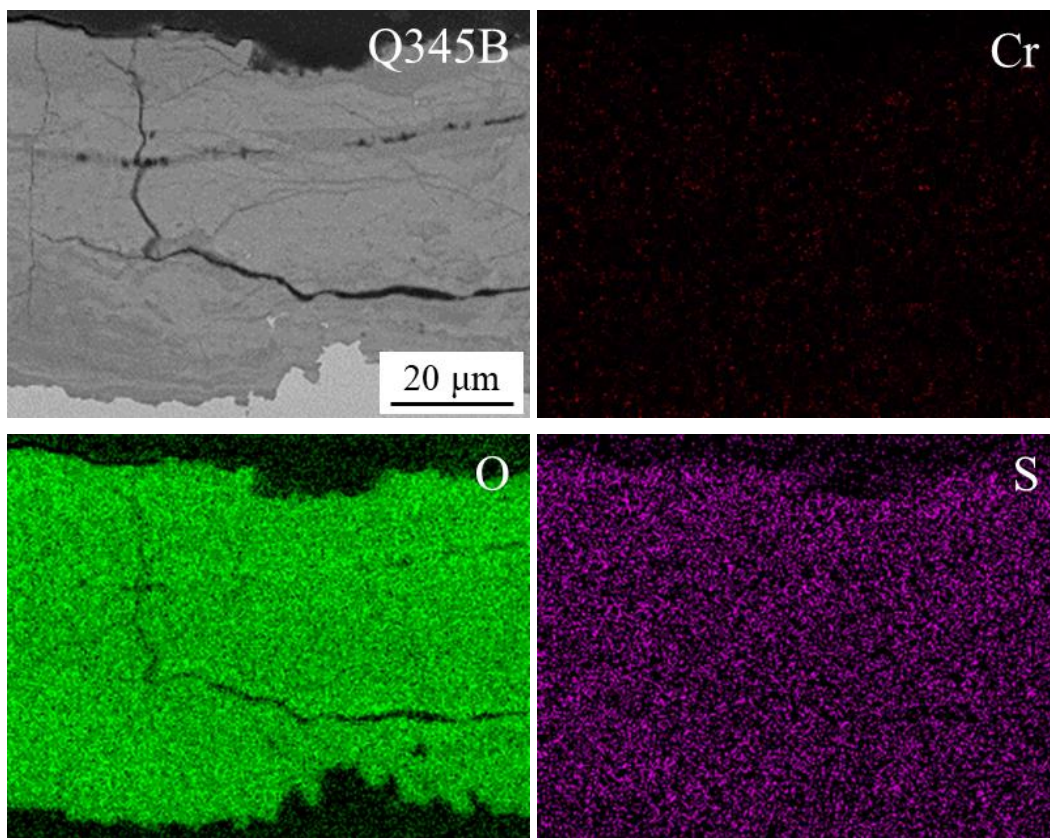
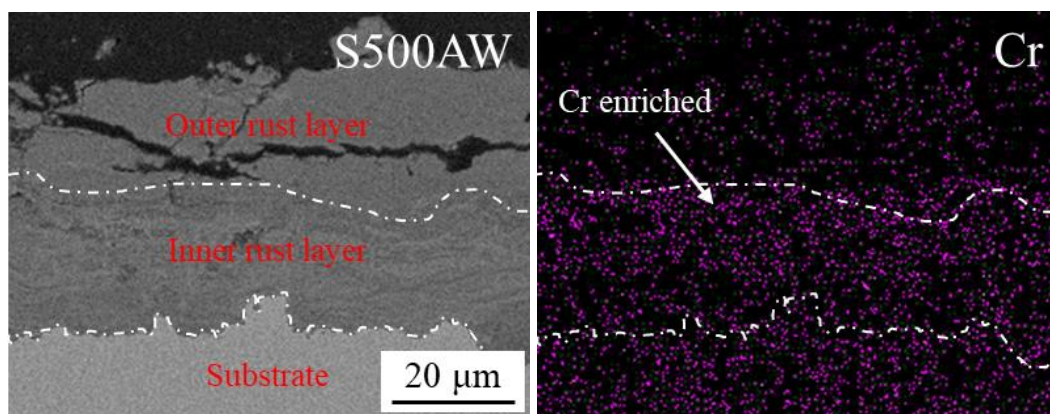


Figure 6 SEM image and element distribution of Q345B carbon steel after 360-h periodic immersion test in 0.01 mol/L NaHSO₃ at 25 °C.



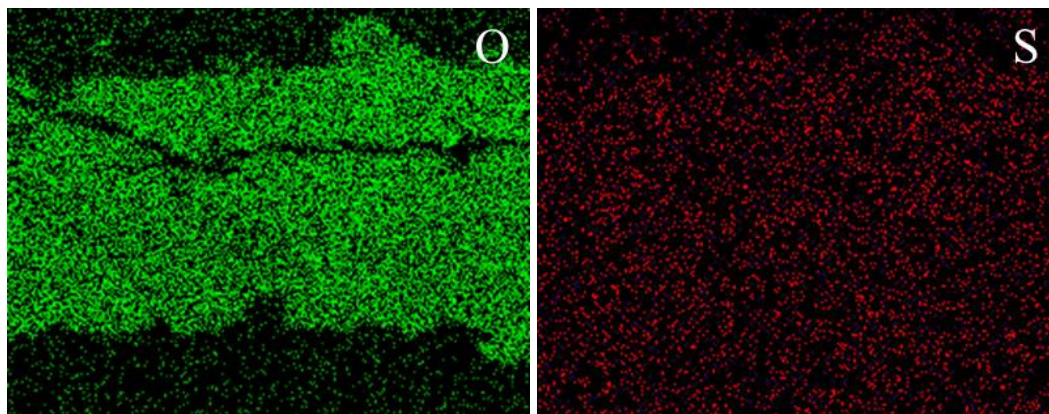


Figure 7 SEM image and element distribution of S500AW railway steel after 360-h periodic immersion test in 0.01 mol/L NaHSO₃ at 25 °C.

3.3 Composition of Corrosion Products

Figure 8 (a) and (b) display the XRD patterns of Q345B carbon steel and S500AW railway steel in 0.01 mol/L NaHSO₃ solution at different periods of the periodic immersion experiments. Figure 9 shows the results of the semiquantitative analysis. The XRD patterns of the two types of steel demonstrate that the corrosion products of the two types of steel are α -FeOOH, γ -FeOOH, Fe₃O₄ and γ -Fe₂O₃, but the peak strengths and widths are different, indicating that the corrosion products of different samples account for different proportions in the rust layer.

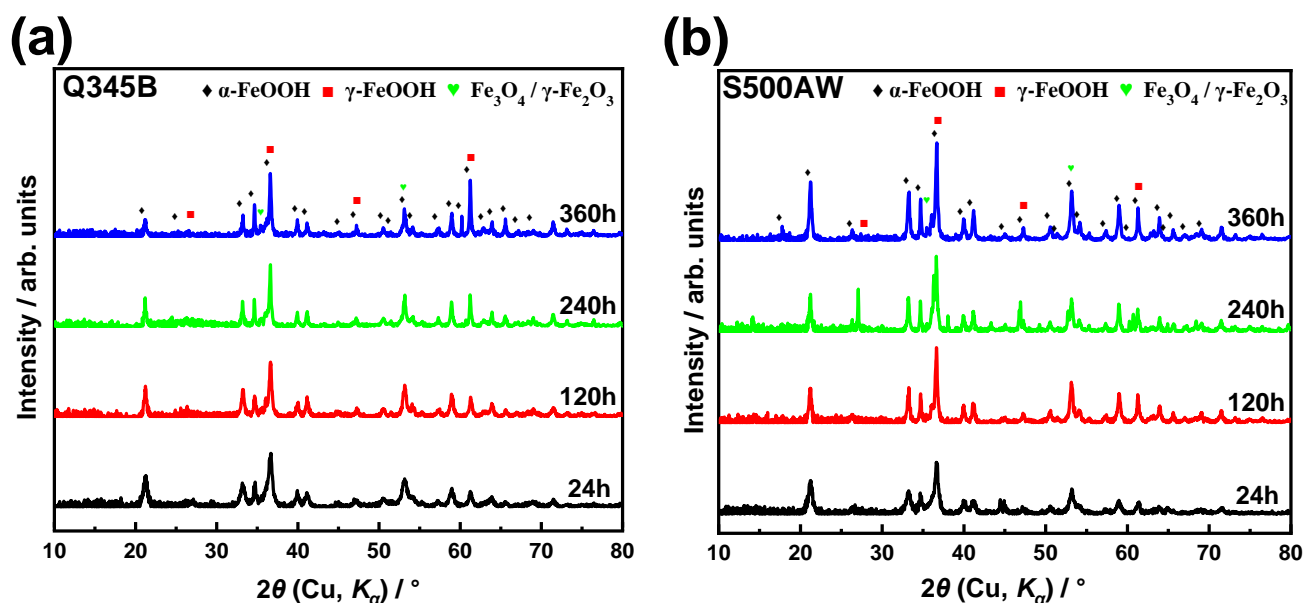


Figure 8 XRD of corrosion products of two steels after cyclic immersion tests in 0.01 mol/L NaHSO₃ solution at 25 °C for different periods: (a) Q345B; (b) S500AW

As seen from Figure 9, α -FeOOH accounts for the largest proportion, followed by γ -FeOOH, and Fe₃O₄ & γ -Fe₂O₃ account for the smallest proportion. γ -FeOOH gradually transforms into α -FeOOH 26-

27, which has stronger thermodynamic stability during periodic immersion experiments. Therefore, with an extension of test times, the proportion of α -FeOOH increases. Antony et al. pointed out the reaction activity sequence of various rust components: α - FeOOH < γ - FeOOH < Fe₃O₄/ α -Fe₂O₃, which implies that α -FeOOH is more defensive to the substrate 28.

The α/γ value of the rust layer was calculated to further investigate the protection ability of the two types of steel. It is commonly considered that the corrosion product layer provides good protection to the substrate when α/γ is greater than 2.0 29. It can be seen from Figure 9 that the rust layers of the two types of steel have better protection performance at 24 h. The α/γ value was increasing, which demonstrated that the rust layer becomes increasingly defensive with the extension of test time. The rust layer of Q345B carbon steel at the early stage of corrosion was higher than that of S500AW railway steel, and the α/γ value reached 8.48 at 120 h. However, the α/γ value changed little after 120 h (9.12 after 360 h) with the extension of the time, which indicated that the transformation amount from γ -FeOOH into α -FeOOH reached its upper limit. The α/γ value of S500AW railway steel was relatively small, but with the extension of the time, γ -FeOOH constantly transformed into α -FeOOH, and the α/γ value continued to increase. In addition, it can be illustrated that in Figure 9, the α/γ value of S500AW, which reached 14.03, was definitely higher than that of Q345B carbon steel at 360 h.

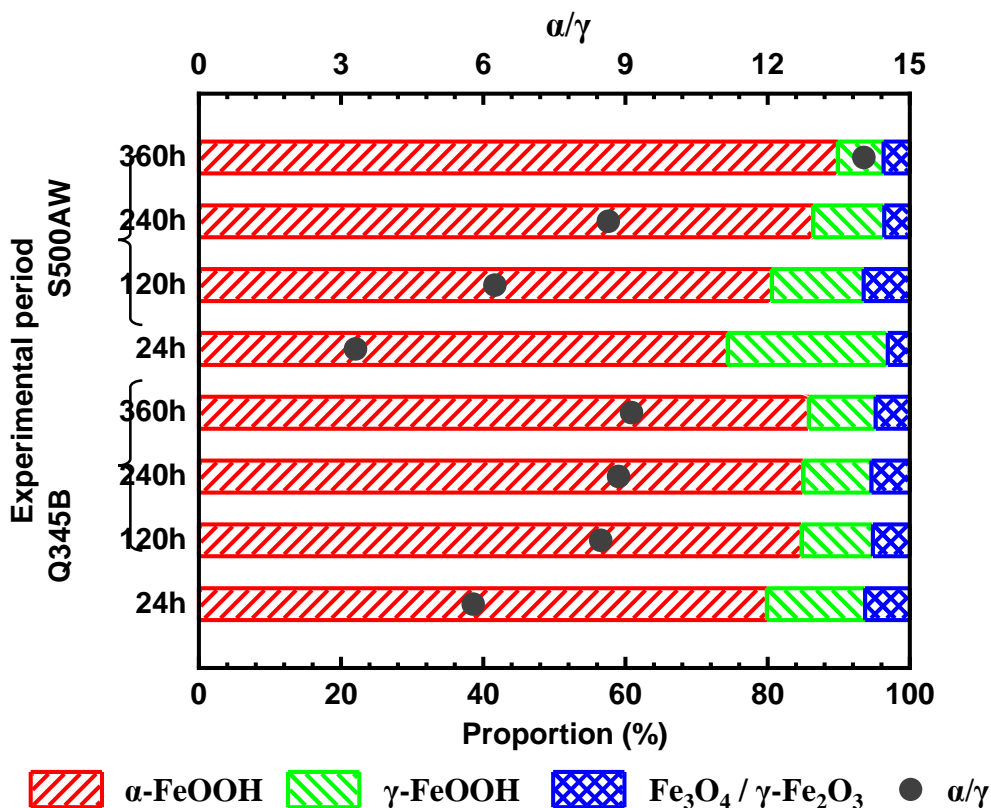


Figure 9 Semiquantitative analysis of XRD results after cyclic immersion tests in 0.01 mol/L NaHSO₃ solution at 25 °C for different periods.

3.4 Polarization Curve Analysis

Figure 10 (a) and (b) show the polarization curves of Q345B and S500AW after periodic immersion experiments in 0.01 mol/L NaHSO₃ solution at different times.

Table 4 presents the Tafel fitting results of the corrosion current density and corrosion potential.

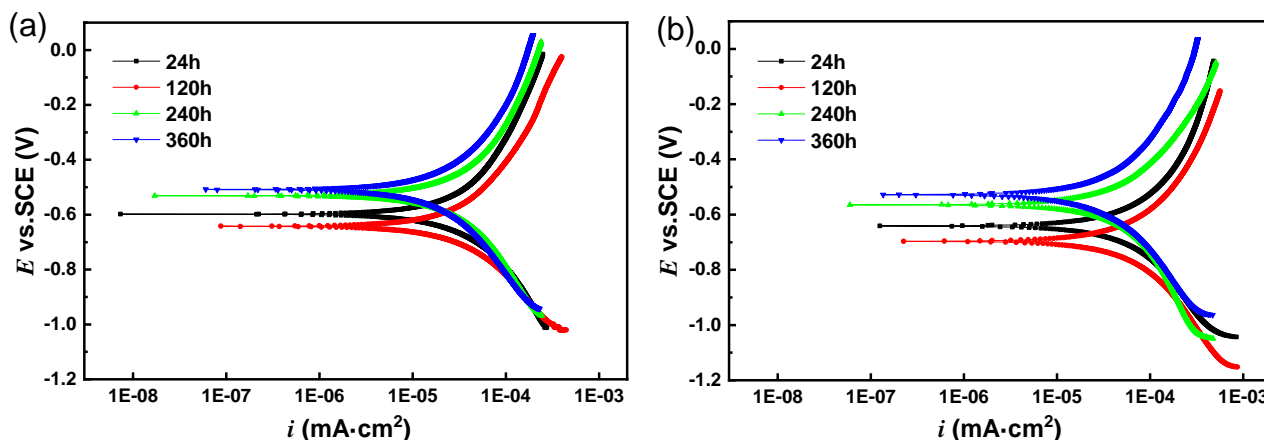


Figure 10 Polarization curves of two steels after periodic immersion tests in 0.01 mol/L NaHSO₃ solution at 25 °C for different periods. (a) Q345B; (b) S500AW

Table 4 Tafel fitting results of Q345B carbon steel and S500AW railway steel after periodic immersion testing in 0.01 mol/L NaHSO₃ solution at 25 °C for different periods.

Experimental period	E_{corr} (mV)		i_{corr} ($\mu\text{A}\cdot\text{cm}^2$)	
	Q345B	S500AW	Q345B	S500AW
24 h	-641.301	-598.066	68.906	39.184
120 h	-696.904	-642.024	88.095	48.959
240 h	-564.537	-531.245	54.903	32.547
360 h	-534.373	-508.990	49.635	28.848

From the polarization curves of Q345B carbon steel in Figure 10 (a), it can be confirmed that the shapes of the anodic polarization curves were smooth and similar, indicating that during the four cycles of periodic immersion experiments, there was a similar corrosion mechanism and no passivation phenomenon, and it was in the activated dissolution state (as shown in Equation 4). However, the anodic polarization curves first shift to the right and then to the left with a change in experimental cycles, indicating that the corrosion current density also increases and then decreases under the same corrosion potential. The cathodic polarization curves included the oxygen absorption reaction (Equation 5) and hydrogen evolution reaction (Equation 6) in the weakly acidic environment of 0.01 mol/L NaHSO₃ solution. With increasing current density, the cathodic polarization curves decreased. The results in Figure 10 (b) are the same for S500AW railway steel.

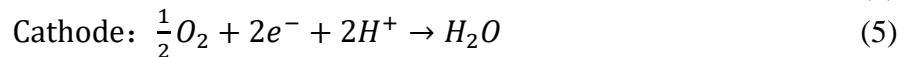


Table 4 shows that when the initial corrosion experiment was conducted for 120 h, the corrosion potential of both types of steel shifted negatively, and the corrosion current density increased correspondingly. The anodic potential of both types of steel presented an increasing trend, which indicated that both Q345B carbon steel and S500AW railway steel display an active dissolution corrosion trend during the periodic immersion experiments, and the corrosion potential and corrosion current density reached a maximum at 120 h. Corrosion was easy to carry out. The D value in the kinetic fitting curves in Figure 1 demonstrated the initial corrosion rate, and the D value of Q345B carbon steel was greater than that of S500AW railway steel, which was consistent with the results of the polarization curve. It can be illustrated from the results in

Table 2 that the corrosion rate of the specimens also reached the maximum value at 120 h. The results obtained from the electrochemical test were in good agreement with the results obtained from the corrosion weight loss experiment at 120 h.

From the middle stage of corrosion to 360 h, the corrosion potential shifted positively, and the corrosion current density decreased, which indicated that it was difficult to corrode in a simulated industrial atmosphere. Relatively fine corrosion products were formed at this stage, which can inhibit the anodic dissolution process of the steel and retard the corrosion of the substrate. In combination with the results of Figure 1 and Table 3, the n value in the kinetic fitting curves was less than 1.0, and the corrosion rate correspondingly decreased with the extension of the experiment times. The results of the electrochemical tests from the middle stage of corrosion to 360 h were in good agreement with those of the corrosion weight loss experiments.

In addition, the corrosion potential of Q345B carbon steel was more negative than that of S500AW railway steel at any time of the periodic immersion experiments, and the corrosion current density was higher, which indicated that S500AW railway steel showed better corrosion resistance.

4. DISCUSSION

The corrosion performance of S500AW railway steel is better than that of Q345B carbon steel in a simulated industrial atmosphere. The dense corrosion products covering the steel surface have a certain shielding effect on the steel. The α/γ value can represent the protection ability of the rust layer [29]. The changing trend of the α/γ value was different with an extension of the experiment time (as shown in Figure 11). The α/γ value of Q345B carbon steel was relatively larger at 24 h, but its growth rate decreased with the expansion of the experiment times and had basically reached the upper limit of growth. Although the α/γ value of S500AW was less than that of Q345B, the value increased swiftly and presented a constantly increasing trend.

The above changes are caused by the acid cycle corrosion mechanism of steel in the simulated industrial atmospheric environment 30, resulting in the acceleration of the corrosion rate at the initial stage (reaching the maximum at 120 h after the test). The corrosion rate of Q345B carbon steel was relatively faster in the early stage. Guo et al. 31 showed that SO₂ can promote the formation of corrosion products α -FeOOH in carbon steel. Therefore, the corrosion products produced in the early stage began to transform into α -FeOOH, while the initial corrosion rate of S500AW railway steel was slow, and the transformation of corrosion products occurred later than that of carbon steel. This explains why the α/γ value of Q345B is greater than that of S500AW at this stage. As corrosion continues, the rising rate of the α/γ value of Q345B decreases gradually, which demonstrates that the transformation quantity of α -FeOOH has reached the upper limit. However, the Cr element added in S500AW can promote the formation of fine α -FeOOH 32, and the Cr enriched in cracks and pores can be incorporated into α -FeOOH to form α -(Fe_xCr_(1-x))OOH 9, so the transformation into α -FeOOH progressively occurred. The α/γ value increased constantly and reached 14.03 at 360 h.

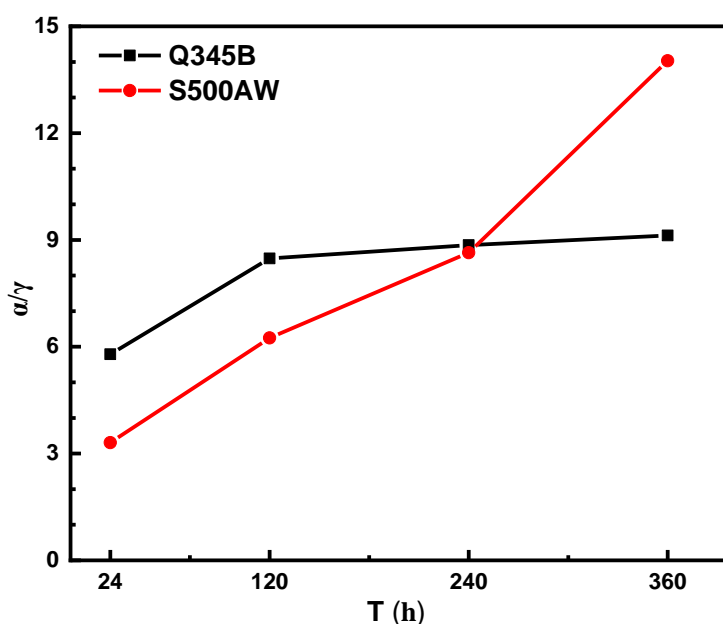


Figure 11 Variation of α/γ values with time of periodic immersion test in 0.01 mol/L NaHSO₃ at 25 °C.

The rust layer of S500AW railway steel had an interior and exterior structure under the simulated industrial atmosphere. The corrosion products of the exterior rust layer were mainly γ -FeOOH, while the corrosion products of the interior rust layer were mainly dense α -FeOOH. The interior layer had a better protective effect. The formation and transformation process of rust layer products of S500AW railway steel are as follows. First, anodic dissolution of Fe occurs to form Fe²⁺. Then, γ -FeOOH is formed through hydrolysis or oxidation. Finally, with the extension of corrosion, α -FeOOH is formed through the process of dissolution and redeposition.

The formation of a rust layer causes a change in the internal stress on the steel surface, so cracks, micropores and other defects are generated on the surface, as illustrated in Figure 12 (a). The shape of γ -FeOOH is scaly 33, causing a loose and porous rust layer and easy invasion of corrosion medium into

the substrate. It can also be illustrated from the cross-section morphology in Figure 6 that there were large longitudinal and transverse cracks and many small microcracks in the rust layer of Q345B carbon steel, and the corrosion medium can invade the interior along with these crack defects. Such a rust layer absorbs water molecules and promotes the transmission of oxygen 18, which further accelerates the corrosion of carbon steel. Based on the above results and Table 2, it was found that the corrosion rate reached a maximum at 120 h in the early stage. In addition, according to the polarization curves in Figure 10 and the Tafel fitting results in Table 4, the corrosion current density was also the maximum at 120 h, so corrosion easily occurred in this stage. Cr is redistributed and enriched in the interior rust layer during corrosion, as illustrated in Figure 12 (b). The interior rust layer promoted by Cr covers the surface of S500AW railway steel and can fill the defects and cracks on the surface of the rust layer (as shown in Figure 5) and enhance the corrosion resistance of steel. As shown in Figure 1 and Table 2, the corrosion rate of S500AW railway steel decreased after 120 h; in addition, the corrosion current density of the polarization curves in Figure 10 and the Tafel fitting results in Table 4 also decreased. Based on the above analysis, the corrosion resistance of S500AW railway steel is better than that of Q345B carbon steel.

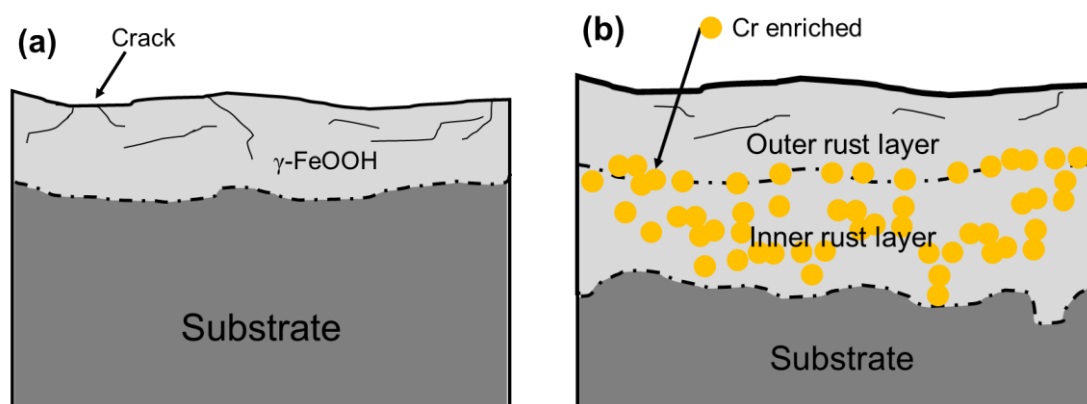


Figure 12 Corrosion mechanism diagrams of S500AW in 0.01 mol/L NaHSO₃ at 25 °C. (a) Corrosion prophase; (b) Corrosion anaphase

5. CONCLUSIONS

The corrosion behaviour of Q345B carbon steel and S500AW railway steel was studied in a 0.01 mol/L NaHSO₃ solution by periodic immersion experiments. The following conclusions can be drawn:

(1) In the simulated industrial atmospheric corrosion environment, the corrosion rate of Q345B carbon steel is greater than that of S500AW railway steel in four test cycles, which is 2.95 times that of S500AW railway steel at 360 h. The atmospheric corrosion resistance of S500AW railway steel is better.

(2) The rust layer of S500AW railway steel is divided into interior and exterior layers. Cr elements are enriched in the interior rust layer, and there are no large or wide cracks in the rust layer of S500AW railway steel.

(3) During 360-h periodic immersion experiments, there was an upper limit to the α/γ value of Q345B but not for S500AW railway steel.

ACKNOWLEDGEMENT

This work was supported by the National Key Research and Development Program of China (Grant No. 2017YFB0304602)

References

1. S. Ding, D. Chen, J. Liu, *Chinese Journal of Theoretical and Applied Mechanics*, 53 (2021) 35.
2. P. Tan, J. Ma, J. Zhou and Y. Fang, *J. Zhejiang Univ.-SCIA*, 17 (2016) 923.
3. X. Jin, *J. Zhejiang Univ.-SCIA*, 15 (2015) 936.
4. X. Guo, Z. Liu, R. Zhang, J. Xing, Z. Jin, A. Sun, *Angang Technology*, 4 (2018) 9.
5. C. He, W. Yu, D. Tang, *Hot Working Technology*, 49 (2020) 15.
6. E. Kusmierek, E. Chrzescijanska, *Data Brief*, 3 (2015) 149.
7. Y. Yin, J. Zhao, X. Cheng, X. Li, *Science & Technology Review*, 30 (2012) 48.
8. Y. Liu, H. Yan, L. Du, *Corros. Eng. Sci. Technol.*, 55 (2022) 159.
9. T. Zhang, W. Liu, Z. Yin, B. Dong, Y. Zhao, Y. Fan, J. Wu, Z. Zhang and X. Li, *J. Mater. Eng. Perform.*, 29 (2020) 2531.
10. Y. Qian, Z. Li, *Baosteel Technology*, 2 (2007) 5.
11. K. Asami, M. Kikuchi. *Corrosion Sci.*, 45 (2003) 2671.
12. J. Fu, S. Wan, Y. Yang, Q. Su, W. Han and Y. Zhu, *Constr. Build. Mater.*, 306 (2021) 124864.
13. Y. Qian, C. Ma, D. Niu, J. Xu and M. Li, *Corrosion Sci*, 74 (2013) 424.
14. X. Zhang, S. Yang, W. Zhang, H. Guo and X. He, *Corrosion Sci*, 82 (2014) 165.
15. Q. Yu, C. Dong, Y. Fang, K. Xiao, C. Guo, G. He and X. Li, *J. Iron Steel Res. Int.*, 23 (2016)1061.
16. W. Liu, J. Liu, H. Pan, F. Cao, Z. Wu, H. Lv and Z. Xu, *J. Alloy. Compd.*, 834 (2020) 155095.
17. Y. Wang, J. Li, Q. Wang and T. Wang, *Corrosion Sci*, 181 (2021) 109322.
18. W. Han, C. Pan, Z. Wang and G. Yu, *J. Mater. Eng. Perform.*, 24 (2014) 864.
19. C. Pan, W. Han, Z. Wang, C. Wang and G. Yu, *J. Mater. Eng. Perform.*, 25 (2016) 5382.
20. Y. Qian, J. Xu and M. Li, *Anti-Corros. Methods Mater.s*, 62 (2015) 77.
21. F. Iwei, *Br. Corros. J.*, 26 (1991) 209.
22. M. Morcillo, S. Feliu and J. Simancas, *Br. Corros. J.*, 28 (1993) 50.
23. J. Tafel, *Zeitschrift für physikalische Chemie*, 50 (1905) 641.
24. J. Li, Z. Zhu, H. Chen, S. Li, H. Wu, X. Gao, L. Du and L. Song, *Appl. Sci.-Basel*, 11 (2021) 8668.
25. M. Yamashita, H. Nagano, T. Misawa and H. E. Twonsend, *ISIJ Int.*, 38 (1998) 285.
26. M. Natesan, S. Selvaraj, T. Manickam and G. Venkatachari, *Sci. Technol. Adv. Mater.*, 9 (2008) 045002.
27. T. Ishikawa, K. Takeuchi, K. Kandori and T. Nakayama, *Colloid Surf. A-Physicochem. Eng. Asp.*, 266 (2005) 155.
28. H. Antony, S. Perrin, P. Dillmann, L. Legrand and A. Chaussé, *Electrochim. Acta*, 50 (2007) 7754.
29. W. Wu, X. Cheng, J. Zhao and X. Li, *Corrosion Sci*, 165 (2020) 108416.
30. C. Pan, M. Guo, W. Han and Z. Wang, *Corros. Eng. Sci. Technol.*, 54 (2019) 241.
31. M. Guo, C. Pan, Z. Wang and W. Han, *Acta Metall. Sin.*, 54 (2018) 65.
32. B. Wang, Z. Liu, J. Chen and Q. Liu, *Materials Protection*, 47 (2014) 61.
33. M. Yamashita, H. Miyuki, Y. Matsuda, H. Nagano and T. Misawa, *Corrosion Sci*, 36 (1994) 283.